International Journal of Heat and Fluid Flow 30 (2009) 1183–1192

Contents lists available at ScienceDirect

International Journal of Heat and Fluid Flow

journal homepage: www.elsevier.com/locate/ijhff

Atomization and spray characteristics of bioethanol and bioethanol blended gasoline fuel injected through a direct injection gasoline injector

Su Han Park, Hyung Jun Kim, Hyun Kyu Suh, Chang Sik Lee *

Department of Mechanical Engineering, Hanyang University, 17 Haengdang-dong, Sungdong-gu, Seoul 133-791, Republic of Korea

ARTICLE INFO

Article history:
Received 10 February 2009
Received in revised form 11 June 2009
Accepted 21 July 2009
Available online 18 August 2009

Keywords:
Atomization
Bioethanol
E85
Linearized instability sheet atomization (LISA) model
Spray tip penetration
Sauter mean diameter (SMD)

ABSTRACT

The focus of this study was to investigate the spray characteristics and atomization performance of gasoline fuel (G100), bioethanol fuel (E100), and bioethanol blended gasoline fuel (E85) in a direct injection gasoline injector in a gasoline engine. The overall spray and atomization characteristics such as an axial spray tip penetration, spray width, and overall SMD were measured experimentally and predicted by using KIVA-3V code.

The development process and the appearance timing of the vortices in the test fuels were very similar. In addition, the numerical results accurately described the experimentally observed spray development pattern and shape, the beginning position of the vortex, and the spray breakup on the spray surface. Moreover, the increased injection pressure induced the occurrence of a clear circular shape in the downstream spray and a uniform mixture between the injected spray droplets and ambient air. The axial spray tip penetrations of the test fuels were similar, while the spray width and spray cone angle of E100 were slightly larger than the other fuels. In terms of atomization performance, the E100 fuel among the tested fuels had the largest droplet size because E100 has a high kinematic viscosity and surface tension.

1. Introduction

Cleaner emissions and improvements of fuel consumption economy with internal combustion engines are important issues considering carbon dioxide exhaust regulations and the limited supply of crude oil. Considering these issues, the development of a gasoline direct injection (GDI) engine is important because it simultaneously has advantages of higher thermal efficiency due to direct fuel injection and higher power output than conventional engines. In addition, a GDI engine can also lead to better transient response, more precise control of the air–fuel ratio, an improvement of fuel economy, and a reduction of exhaust emissions because ultra lean combustion due to stratification and a rich fuel–air mixture near the spark plug is possible. In addition, an increase of the compression ratio due to the reduced possibility of knocking leads to an improvement of the output performance (Zhao et al., 1999). For these reasons, an understanding of the spray, the atomization characteristics of fuels, and the complicated and various physical chemistry phenomena in the direct injection gasoline engine is very important to optimize the GDI combustion system. Therefore, many researchers have actively studied the GDI engine and its optimization.

Lee et al. (2001a) studied the spray structure characteristics of a high pressure gasoline injector. They revealed that the GDI injector produced a hollow-cone spray due to the centrifugal force resulting from the angular momentum generated at tangential ports in the nozzle. In addition, they reported that the upward spray vortex contributed to a uniform distribution of fuel droplets. Wang et al. (2005) reported that the GDI spray can be divided into an initial spray stage (initial spray slug) and a main spray stage. In their paper, the initial spray slug generated due to low overall injection and tangential speeds is the remnant fuel of the early injection cycle in the slots between the needle and the tangential gap. The main spray has a hollow cone structure with a distinct swirl structure occurring on both sides of the spray, leading to strong air entrainment and fuel air mixing. Vita and Allocca (2003) verified and improved a numerical method (KIVA-3V code) for analysis of the direct injection gasoline spray characteristics. Kawahara et al. (2004) observed and analyzed the fuel spray behavior near the nozzle tip of a GDI injector. They revealed that the liquid film sheet has a ligament structure and a higher injection pressure causes reduced thickness and a shorter length of the liquid sheet. In addition to these mentioned studies, many researches regarding GDI engines have performed (Lee et al., 2001b; Powell and Lee, 2007). In particular, spray-guided GDI engines are currently being actively investigated (Chang et al., 2007; Kim et al., 2008).

Ethanol fuel and ethanol blended gasoline fuels (E100, E85, etc.) are used in many countries as alternative fuels to gasoline due to

* Corresponding author. Tel.: +82 2 2220 0427; fax: +82 2 2281 5286.
E-mail address: cslee@hanyang.ac.kr (C.S. Lee).

0142-727X/$ - see front matter © 2009 Elsevier Inc. All rights reserved.
doi:10.1016/j.ijheatfluidflow.2009.07.002

Nomenclature

d_D	droplet diameter (mm)	P_{amb}	ambient pressure (MPa)
d_L	ligament diameter (mm)	P_{inj}	injection pressure (MPa)
D	nozzle diameter (mm)	t_{eng}	energizing duration (ms)
h	sheet half wavelength (μm)	μ, μ_l	dynamic viscosity (cP)
K_S	wavelength	ν	kinematic viscosity (mm^2/s)
K_L	most unstable wavelength	ρ, ρ_l	density (kg/m^3)
$L_{breakup}$	ligament breakup length (cm)	σ, σ_l	surface tension (dyn/cm)
U	total sheet velocity (m/s)	Ω	maximum growth rate
V	velocity (m/s)		

issues with the exhaust gas of traditional gasoline. Ethanol fuel can be produced by bio-technology processes utilizing plant material such as corn, sweet potatoes, and tree trunks. Gao et al. (2007) studied the spray characteristics using ethanol–gasoline blended fuels. They reported that the main spray tip penetration decreases and the spray cone angle increases with the increase of the ethanol fraction in the low ambient pressure. However, in the case of the elevated ambient pressure conditions, the difference of spray penetration among the blends shows inconspicuous, while the spray cone angle of all test fuels keeps almost constant in the fully developed stage except that the spray of pure gasoline shows a larger spray cone angle in the beginning of injection period. Aleiferis et al. (2008) studied the spray development and combustion of blends of gasoline, iso-octane and ethanol under part-load engine operation with port fuel injection and direct injection in an optical spark-ignition engine. An outstanding conclusion in their research is as following. The spray images indicated that a small portion of a low boiling point component in blended fuel may be the catalyst to spray collapse, even if the majority constituent of the fuel is not in the region of flash boiling in terms of temperature. Ethanol fuel containing oxygen molecules has a high combustion efficiency and low pollutant emissions. Despite the advantages of ethanol fuel, the studies of the application of ethanol fuel in GDI engines are insufficient compared to port injection gasoline engines.

The aim of this work was to study the macroscopic and microscopic atomization characteristics of bioethanol and bioethanol blended gasoline fuel by investigating the spray evolution process, overall spray characteristics, and mean droplet size in a direct injection gasoline injector of a gasoline engine. In addition, the spray and atomization characteristics were compared with the numerical results obtained from using the KIVA-3V code.

2. Experimental setup and procedure

2.1. Experimental setup

The schematic of the high pressure swirl injector used in this work is illustrated in Fig. 1a. This injector has a nozzle exit orifice diameter of 1.0 mm and is operated by varying electric voltages. The high pressure swirl injector has a conical type air core at the center axis in the nozzle and it is possible to atomize at a lower injection pressure compared to a conventional port fuel injector. The injection timing and energizing duration of the test injector were controlled by an injector driver (TEMS, TDA-3200H) and a digital delay/pulse generator (Berkeley Nucleonics Corp., Model 555).

In order to investigate the overall spray characteristics of the test fuels including the axial spray tip penetration, spray width,

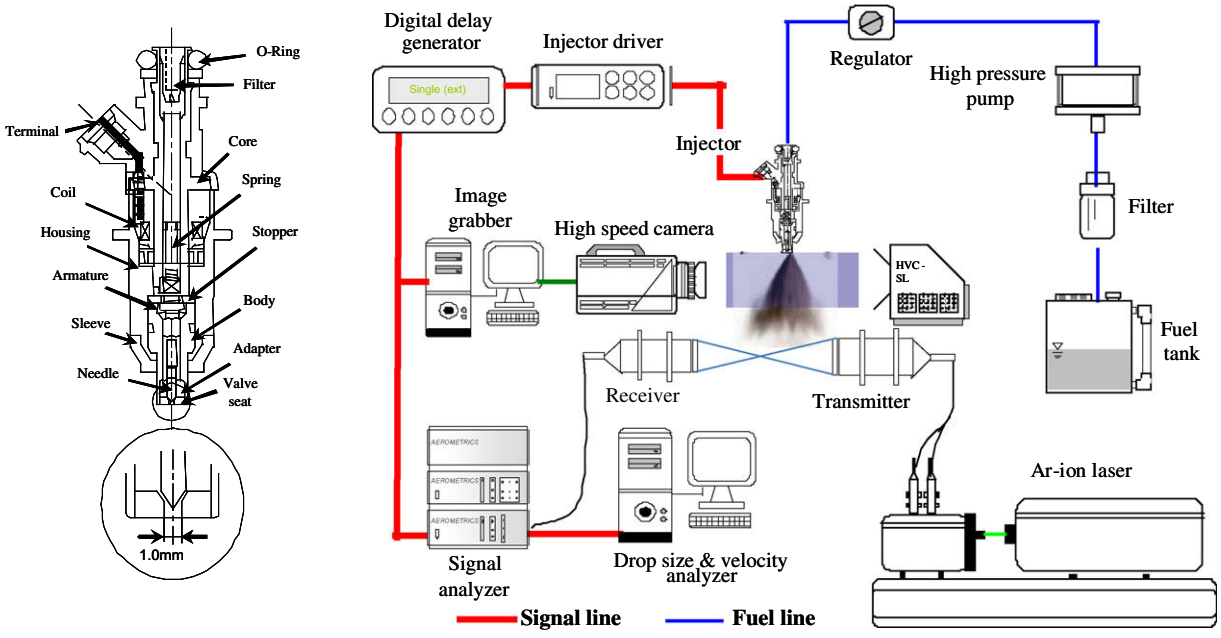

(a) Test injector (b) Visualization and droplet measuring system

Fig. 1. Schematic of test injector and visualization and droplet measuring systems.

Table 1
Specifications of the droplet analysis system and high speed camera.

Visualization system	Frame rate	10,000 fps
	Shutter speed	1/20,000 s
	Resolution	512 × 512
PDPA system	Light source	Ar–ion laser
	Wave length	514.5 nm, 488 nm
	Focal length	500 mm for transmitter and receiver
	Collection angle	30°
	Burst threshold	0.5 mV
	Mixer frequency	36 MHz
	Filter frequency	40 MHz
	PMT voltage	500 V
	Signal-to-noise ratio	65
	Diameter sub-range	1.5–75 μm

spray cone angle, and droplet size, the visualization and droplet analysis system (phase Doppler particle analyzer, PDPA) was installed as shown in Fig. 1b. Spray evolution images were obtained using a high speed camera (Photron, Fastcam-APX RS) with two metal halide lamps. Moreover, the high speed camera was synchronized with the injector driver by using the digital delay/pulse generator and the obtained images were stored in a computer with an image grabber. The frame rate of the high speed camera was maintained at 10,000 fps (frames per second). The droplet analysis system using an Ar–ion laser as a light source consists of a receiver, a transmitter, and a data processing system. The 2-dimensional traverse allows measurements at various measuring points. The detailed specifications of the high speed camera and the droplet analysis system are shown in Table 1.

2.2. Experimental procedure

In this work, the spray and atomization characteristics of a 99.9% pure bioethanol fuel, gasoline fuel, and E85 fuel blend (85% bioethanol + 15% gasoline) were studied. Experimental results of the test fuels were compared with the numerical results obtained from using the KIVA-3V code. The macroscopic spray characteristics including axial spray tip penetration, spray width, and spray cone angle are shown in Fig. 2a. The axial spray tip penetration and spray width were defined as the maximum distance from the nozzle tip of the side view spray image and the maximum radial distance of the bottom view, respectively. Also, the spray cone angle is defined as the interval angle which is formed by the nozzle tip and two straight lines wrapped with the maximum outer side of the spray. Fig. 2b shows the measuring points for analyzing the atomization characteristics of the G100, E100, and E85 fuels.

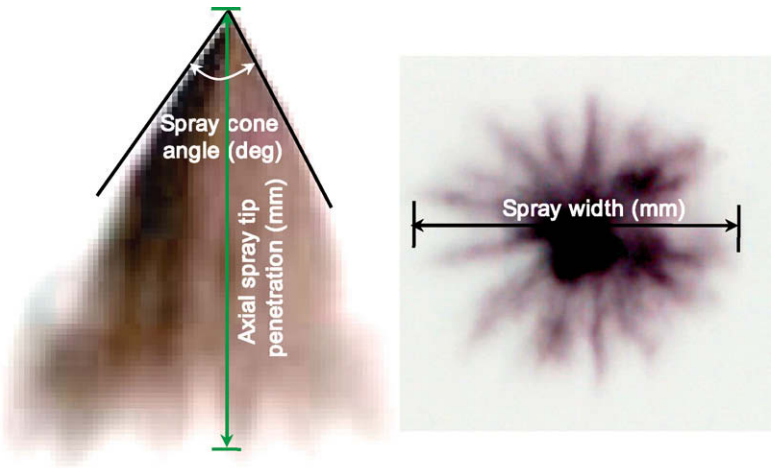

(a) Definition of the spray characteristics (spray tip penetration, spray cone angle, spray width)

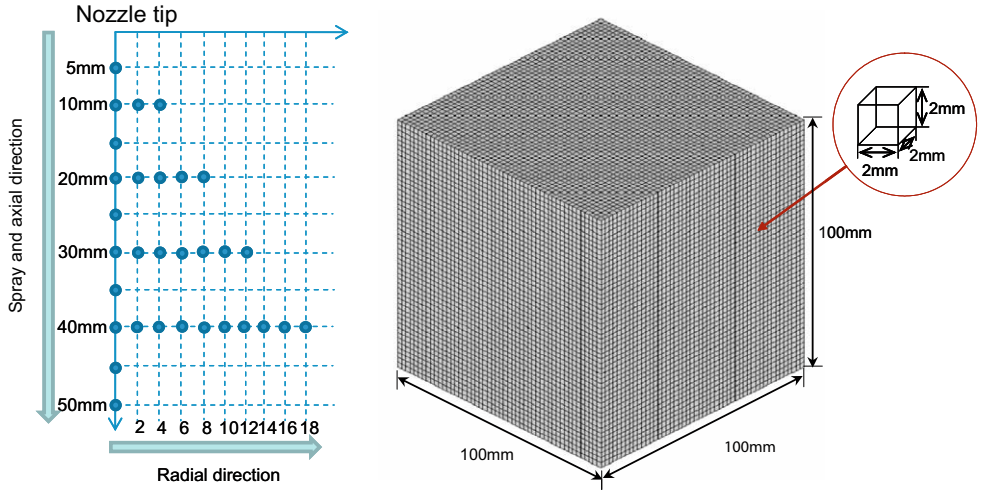

(b) Measuring points for analyzing the atomization characteristics and the calculation meshes

Fig. 2. Definition of spray characteristics, measuring points for the analysis of fuel droplets and the calculation meshes in the KIVA code.

The injection pressure for analyzing the macroscopic spray characteristics was varied among 4.0 MPa, 6.0 MPa, and 8.0 MPa, and the injection pressure for analyzing the atomization performance was set at 7.0 MPa. The comparison of fuel properties and detailed experimental conditions are listed in Tables 2 and 3, respectively.

3. Numerical model formulation for gasoline direct injection

In order to apply the spray of gasoline and bioethanol fuels to the KIVA-3 V code, gasoline (C_8H_{17}) and ethanol (C_2H_5OH) fuel properties from the fuel library (Amsden, 1993) were used to calculate the gasoline (G100) and bioethanol (E100) sprays. In the case of the bioethanol blended gasoline fuel (E85), the fuel library was created on the basis of measured fuel properties such as surface tension, density, and kinetic viscosity, as shown in Table 2. Therefore, the calculations of the spray characteristics injected through the GDI injector were conducted after the fuel library of the test fuel was added and modified in the KIVA-3V code.

In this work, the linearized instability sheet atomization (LISA) model was used for analyzing the gasoline and bioethanol spray at the swirl type GDI injector. This model was purposed by Schmidt et al. (1999) and has been widely used to simulate hollow-cone sprays (Senecal et al., 1999; Lee et al., 2004; Lucchini et al., 2005). The LISA model consists of three stages: film formation, sheet breakup, and atomization. The film formation considers the air core created by the centrifugal motion into the injector and the mass flow rate, total velocity, and velocity coefficient were calculated in this stage. The sheet breakup stage describes the breakup of the liquid sheet due to effects of the surrounding gas, liquid viscosity, and surface tension. The sheet breakup occurs after the unstable waves reach a critical amplitude. The drop size of the ligament was determined from the primary breakup process. The breakup length (L_{breakup}) of the ligament and droplet diameter (d_D) after the breakup was formulated in the paper of Schmidt et al. (1999) as follows

$$L_{\text{breakup}} = \frac{U}{\Omega} \ln\left[\frac{\eta_b}{\eta_0}\right] \tag{1}$$

$$d_D = \left[\frac{3\pi d_L^2}{K_L}\right]^{1/3} \tag{2}$$

Here U and Ω are the total sheet velocity and the maximum growth rate, respectively. The value of $\ln(\eta_b/\eta_0)$ was set at 12 considering Dombrowski and Johns's suggestion (Dombrowski and Johns, 1963). In addition, the diameter of the ligament (d_L) and the most unstable wavelength on the ligament (K_L) were also determined in the paper of Schmidt et al. (1999).

Table 3
Experimental conditions.

Visualization	Injection pressure (P_{inj}, MPa)	4, 6, 8
	Ambient pressure (P_{amb}, MPa)	0.1
	Energizing duration (t_{eng}, ms)	2
PDPA	Injection pressure (P_{inj}, MPa)	7
	Ambient pressure (P_{amb}, MPa)	0.1
	Energizing duration (t_{eng}, ms)	2.0

$$d_L = \left[\frac{16h}{K_s}\right]^{0.5} \tag{3}$$

$$K_L = \frac{1}{d_L}\left[\frac{1}{2} + \frac{3\mu_l}{2(\rho_l \sigma_l d_L)^{1/2}}\right]^{-1/2} \tag{4}$$

Here h and K_s indicate the half thickness of the sheet and the wave number corresponding to the maximum growth rate, respectively. In the atomization stage, the Taylor analogy breakup (TAB) model (O'Rourke and Amsden, 1987) was used to analyze the secondary breakup based on the droplet diameter in the sheet breakup stage.

The calculation conditions used were the same as the experimental conditions shown in Table 3. The total number of injected droplets was set at 5000. The spray angle and duration of pre-spray with nozzle hole diameter were determined to be 10° of a solid cone form and 0.1 ms before the conversion of the hollow cone, respectively. In order to analyze the spray characteristics, uniform cubic meshes with a computational cell size of 2 × 2 × 2 mm were used, as illustrated in Fig. 2b.

4. Results and discussions

4.1. Fuel properties and injection quantity

In this work, fuel properties including fuel density, kinematic viscosity, and surface tension were measured using a hydrometer, a viscometer, and a surface tension meter, respectively, as shown in Fig. 3. Upon increasing the blending ratio of the bioethanol fuel, the properties of the three fuels also increased, nearly linearly. These results were caused by the bioethanol fuel which has higher fuel density, kinematic viscosity, and surface tension values.

Fig. 3 shows the injection quantities for various injection pressures and energizing durations. The energizing duration is defined as the time that the current signal from the injector driver is transmitted to the test injector. As shown in Fig. 3, the injection quantities at an energizing duration of 1.0 ms were nearly uniform, regardless of the increase of the injection pressure. It can be

Table 2
Comparison of fuel properties.[b]

Characteristics	Bioethanol (E100)	Gasoline (G100)	Blend (E85)
Chemical formula	C_2H_5OH	C_4 to C_{12} chains	[a]
Main constituents (% by weight)	C: 52	C: 85∼88	C: 57
	H: 13	H: 12∼15	H: 13
	O: 35	O: 0	O: 30
Fuel density (kg/m^3 @20 °C)	789.67	718.33	778.33
Kinematic viscosity (mm^2/s @20 °C)	1.57	0.84	1.42
Surface tension (N/m @20 °C)	0.027	0.024	0.026
Octane	98∼100	86∼94	105
Lower heating value (MJ/kg)	26.8	41.9∼44.2	29.1
Reid vapor pressure (kPa)	15.8	55.2∼103.4	41.4∼82.7
Ignition point – Fuel in air (%)	3∼19	1∼8	[a]
Stoichiometric air/fuel ratio (by weight)	9	14.7	10
Blending ratio (%)	Bioethanol 100%	Gasoline 100%	Bioethanol 85% Gasoline 15%

[a] Depends on percentage and type of the hydrocarbon fraction.
[b] Handbook for handling, storing, and dispensing E85, U.S. Department of Energy, Energy Efficiency and Renewable Energy, July 2006, DOE/GO-102006-2343.

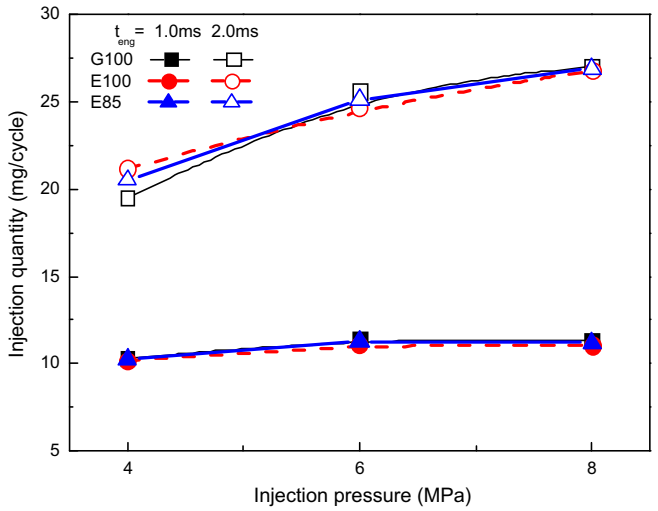

Fig. 3. Injection quantities of test fuels for the injection pressure and energizing duration (P_{inj} = 4.0 MPa, 6.0 MPa, 8.0 MPa, P_{amb} = 0.1 MPa, t_{eng} = 1.0 ms, 2.0 ms).

concluded that the spray momentum at the nozzle exit was not affected much by the increase of the injection pressure, because the injector needle is not fully opened. In addition, the injection quantities at an energizing duration of 2.0 ms increased with the increase of the injection pressure. Therefore, an energizing duration greater than 1.0 ms is needed to fully open the injector needle. Hence, the energizing duration for the visualization and droplet analysis was set at 2.0 ms in this work. The injection quantities of G100, E100, and E85 showed similar increasing patterns and values as the injection pressure and energizing duration increased.

4.2. Spray evolution progress of bioethanol blended gasoline fuel

Fig. 4 shows the spray evolution progresses at the side and bottom views at various elapsed times. As shown in Fig. 4, the initial spray slug which is the remnant fuel of the early injection cycle in the slots between the needle and tangential gap was observed at the early injection stage. This is the reason why the injected spray in the early injection stage has a small tangential velocity and the overall spray velocity is very low. Therefore, the injected fuel droplets in this stage move downstream and consist of large droplets with poor atomization. On the other hand, as shown in Fig. 4, the three test fuels have an upward ring shaped vortex in the outer region in the lower part of the spray 1.1 ~ 1.2 ms after the energizing start due to the difference of pressure by the relative velocity between the injected spray and ambient gas. The upward ring shaped vortex became enhanced as time elapsed. The spray evolution patterns of the G100, E100, and E85 fuels at the side and bottom views were very similar. At the bottom view of the spray, the spray width and area increased as the elapsed time increased and the concentration of the inner spray region increased by the effect of the upward ring shaped vortex. The upward ring shaped vortex moved the fuel droplets from the outer region to the inner region. Therefore, the spray vortex affects the formation of a uniform distribution of fuel droplets.

Fig. 5 shows the comparison of experimental and numerical results of the spray development process for the test fuels under various injection pressures. The numerical results accurately predicted the experimentally observed spray development pattern, shape, the beginning position of the vortex, and spray breakup on the spray surface. As illustrated in Fig. 5, the downstream spray became circular with an increase of the injection pressure. The increase of the injection pressure induced an increase of the relative velocity between the injected spray and ambient gas. Simultaneously, the momentum exchange between the air inside the hollow cone and the injected spray droplets actively progressed. As the velocity of air increases, the static pressure inside the hollow cone of the spray decreases according to the Bernoulli equation. For these phenomena, the droplets of the injected spray moved to the inside of the hollow cone. This results in the circular shape of the spray downstream and the uniform mixture distribution. Therefore, it can be said that the increase of the injection pressure produces a uniform mixture of the injected spray and ambient air.

Fig. 6 shows the overall spray characteristics including the axial spray tip penetration, spray width, and spray cone angle. As shown in Fig. 6, the test fuels have almost the same injection delay of about 0.4 ms, defined as the time interval between the start of the energizing and the initial injected spray. The pre-spray (spray slug) of E100 is longer than G100 and E85 because the E100 fuel has a lower vapor pressure than the G100 and E85 fuels. The pre-spray and main spray curves of the test fuels were nearly identical, as illustrated in Fig. 6a. It can be confirmed that the difference of the fuel properties did not affect the axial spray tip penetration. The spray width and spray cone angle were measured from the start of the main spray. The spray width and spray cone angle of E100 were slightly larger than those of the other fuels, despite the fact that the G100 fuel has a higher vapor pressure. Because gasoline fuel is a mixture of many components with various carbon

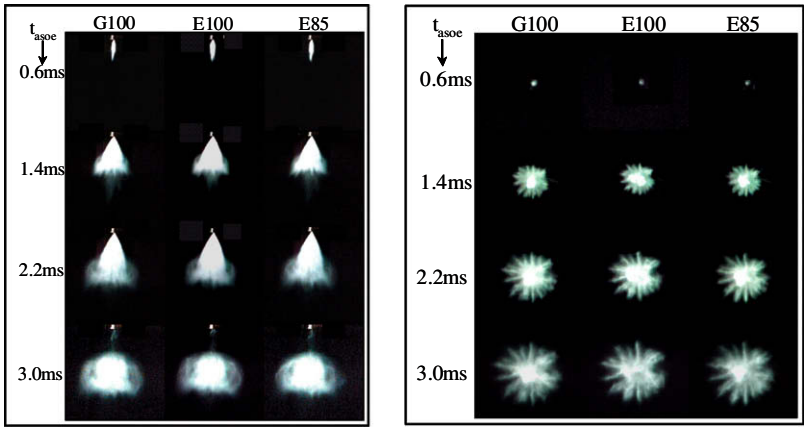

(a) Side view (b) Bottom view

Fig. 4. Spray evolution progress of side view and bottom view (P_{inj} = 6.0 MPa, P_{amb} = 0.1 MPa, t_{eng} = 2.0 ms).

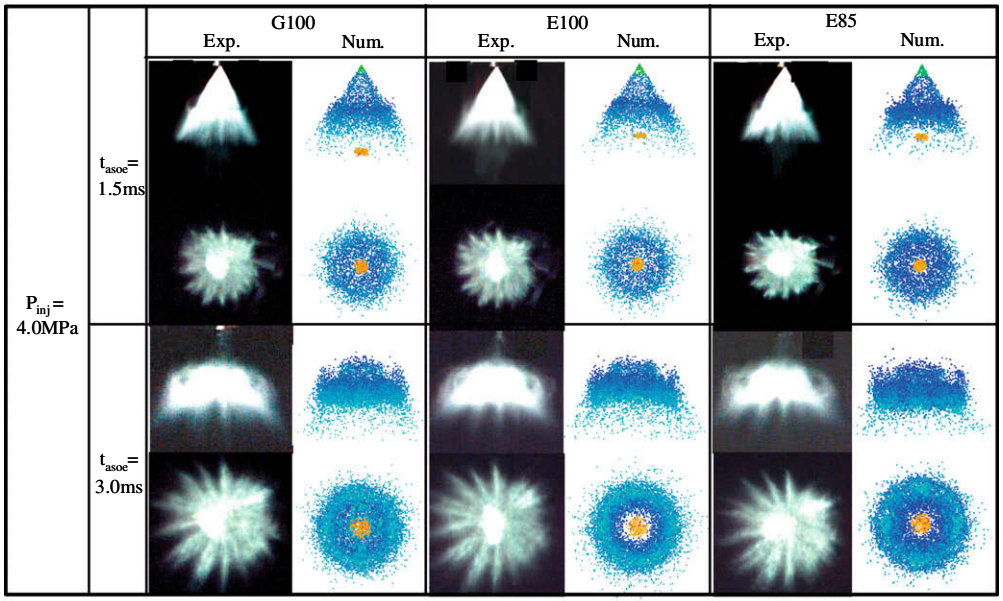

(a) P_{inj}=4.0MPa

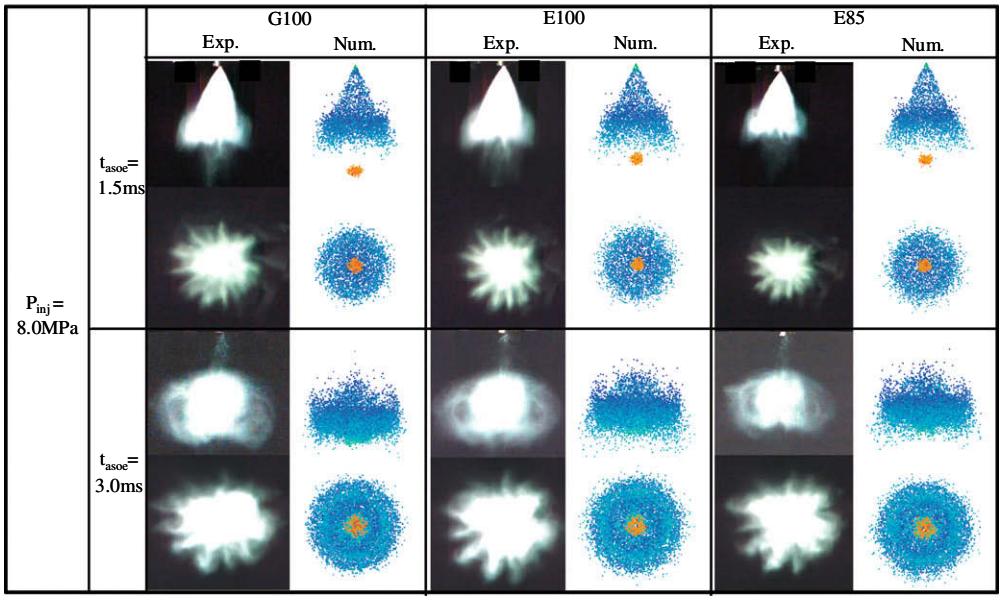

(b) P_{inj}=8.0MPa

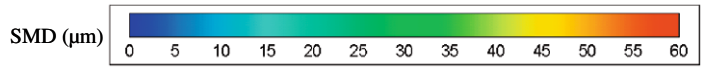

Fig. 5. Comparison between experimental and numerical spray images as a side and bottom view.

atoms and structures, its vapor pressure is largely affected by components with relatively low boiling points which evaporate easier and faster, while the components with higher boiling points will evaporate more slowly. In addition, the spray cone angle was almost uniform during the injection period, while it decreased after the end of the main spray. This is the reason why the transferred spray momentum from the injector stopped and the injected spray evaporated.

Figs. 7 and 8 show the effects of the injection pressure on the axial spray tip penetration and spray cone angle, respectively, with respect to the elapsed time. The injection pressure of the fuel is an important factor which affects the spray evolution process involving the axial spray tip penetration, spray width, spray cone angle, and the mixing of fuel droplets and ambient air. The axial spray tip penetration increased with an increase of the injection pressure. The axial spray tip penetration and spray cone angle of the three fuels were very similar trends. The spray cone angle decreased after the end of the injection as shown in Fig. 6c. After the end of the injection, the spray cone angle of the injected spray showed a large rate of reduction because of rapidly ceasing of injection momentum of liquid spray. Fig. 8 shows the effect of injection pressure on the spray cone angle of three

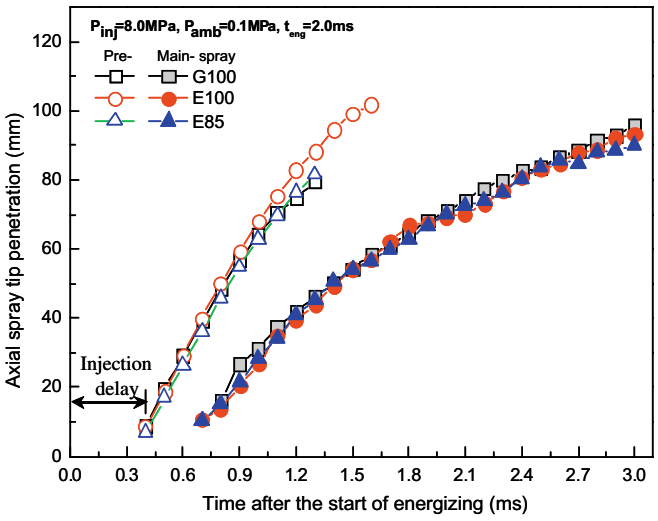

(a) Axial spray tip penetration

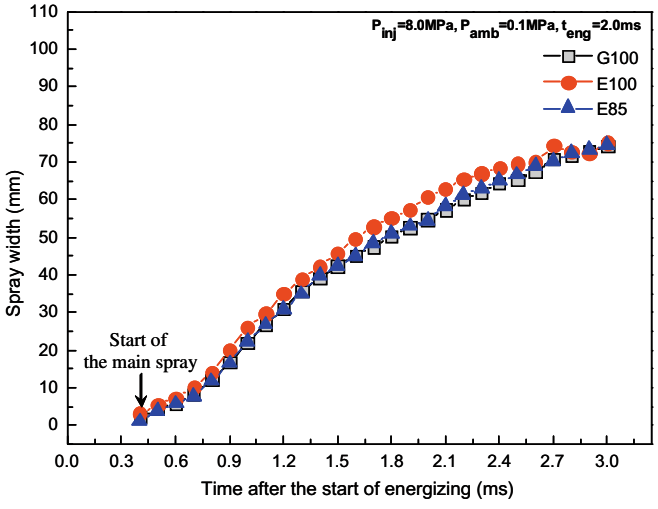

(b) Spray width

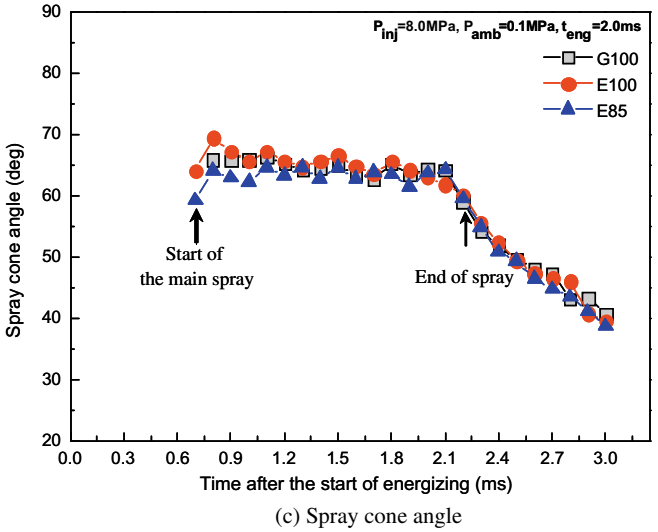

(c) Spray cone angle

Fig. 6. Overall spray characteristics of G100, E100, and E85 (P_{inj} = 8.0 MPa, P_{amb} = 0.1 MPa, t_{eng} = 2.0 ms).

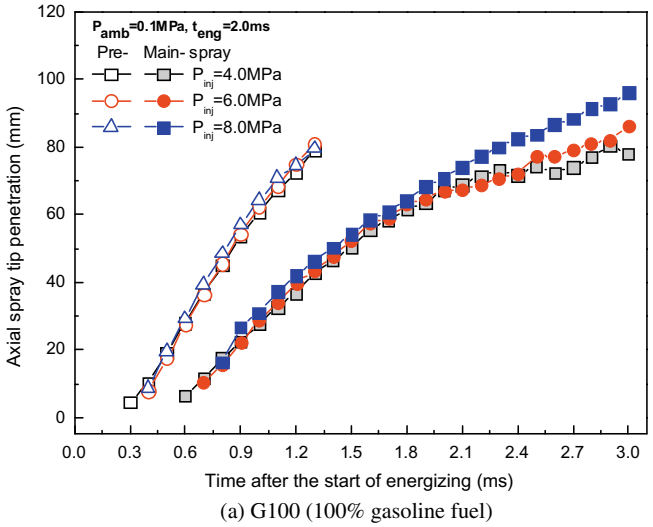

(a) G100 (100% gasoline fuel)

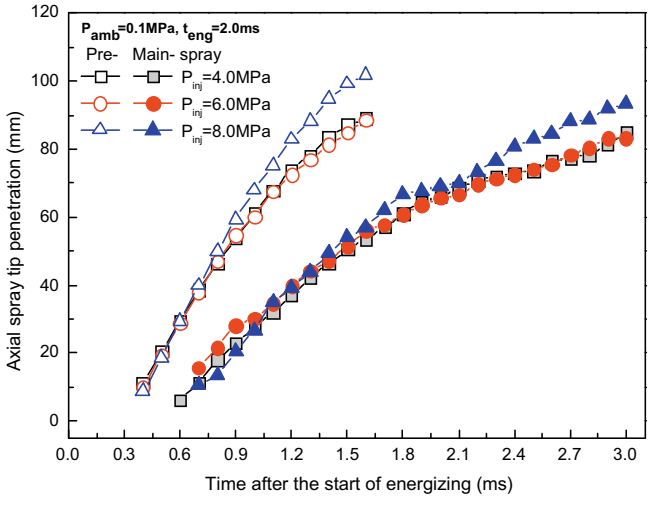

(b) E100 (100% bioethanol fuel)

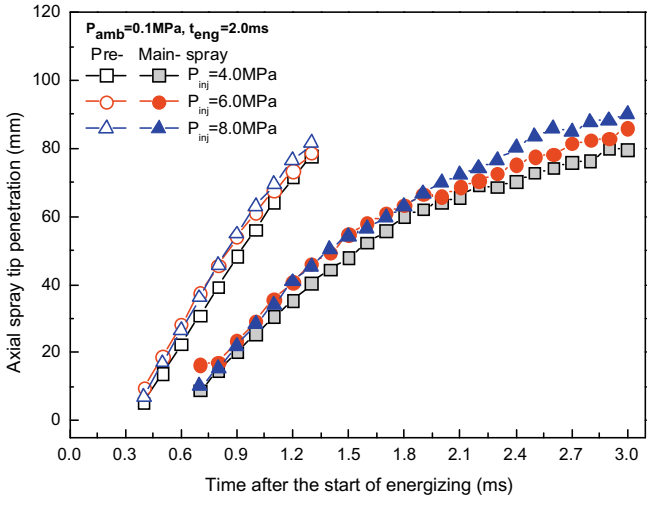

(c) E85 (15% gasoline fuel + 85% bioethanol fuel)

Fig. 7. Effect of the injection pressure on the axial spray tip penetration of test fuels (P_{inj} = 4.0 MPa, 6.0 MPa, 8.0 MPa, P_{amb} = 0.1 MPa, t_{eng} = 2.0 ms).

fuels. As the injection pressure increased, the reduction of cone angle remarkably decreased because the large relative axial velocity due to the high injection pressure caused an enhancement of the axial mixing flow between the injected spray and ambient air. In addition, the strong vortex and large relative

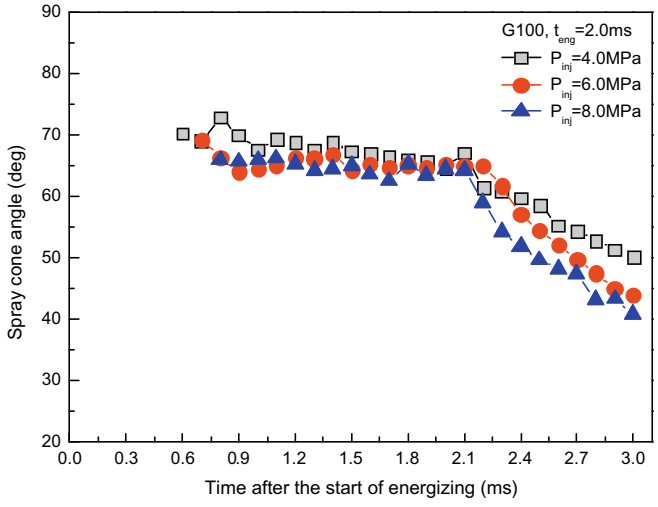

(a) G100 (100% gasoline fuel)

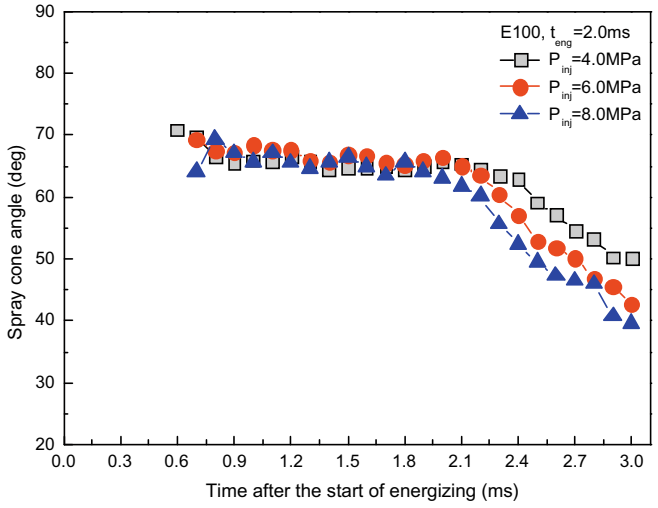

(b) E100 (100% bioethanol fuel)

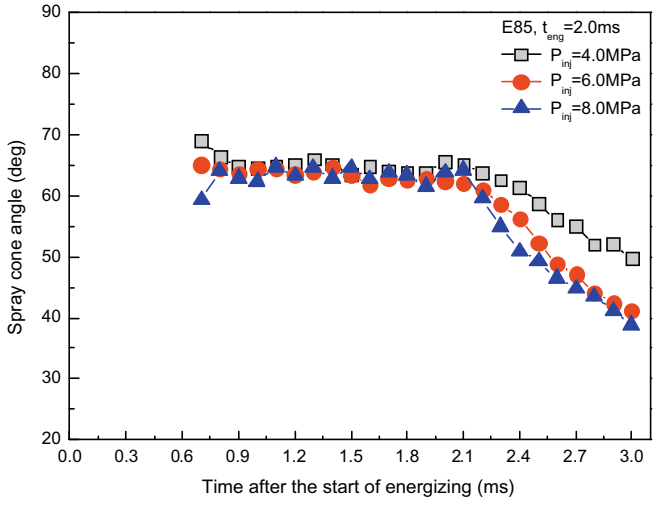

(c) E85 (15% gasoline fuel + 85% bioethanol fuel)

Fig. 8. Effect of the injection pressure on the spray cone angle of test fuels (P_{inj} = 4.0 MPa, 6.0 MPa, 8.0 MPa, P_{amb} = 0.1 MPa, t_{eng} = 2.0 ms).

velocity caused the injected spray droplets to move into the hollow cone.

4.3. Fuel atomization characteristics – Local SMD and overall SMD

Unlike with port injection gasoline engines, fuel atomization characteristics such as the fuel droplet size evolution are important factors to improve the combustion and emission performance of a GDI engine.

Fig. 9 shows the comparison of the overall SMD evolution, which is the time dependant droplet size at whole measuring points, between the experimental and numerical results. Excluding the maximum values, the distribution ranges of G100, E100, and E85 were 16.3–21.3 μm, 16.8–25.8 μm, and 15.9–23.9 μm, respectively. E100 had a wider and higher droplet size region than the G100 and E85 fuels. In the comparison between the experimental and numerical results, the calculated SMD is generally lower than the experimental SMD. It can be explained that the injection velocity in LISA model is determined by the pressure difference, liquid density and velocity coefficient and then fixed. For it, the calculated injection velocity is high compared to the experimental injection velocity. Therefore, the low droplet size was calculated due to the high injection velocity. Moreover, the fuel composition in the fuel library of the numerical analysis tool does not agree perfectly with the real gasoline composition.

The droplet size distributions at specific positions of the G100, E100, and E85 fuels are illustrated in Fig. 10. The droplet sizes of the test fuels decreased after the maximum value near the nozzle exit of the GDI injector. Then, the three test fuels had nearly uniform droplet sizes beyond 20 mm from the nozzle tip. The droplet size of E100 was the largest among the test fuels. This is the reason why the E100 fuel has a high kinematic viscosity, as shown in Table 2. In addition, E100 has the smallest Reynolds number $\left(\mathrm{Re} = \frac{\rho VD}{\mu} = \frac{VD}{\nu}\right)$ assuming that the injected velocity and nozzle diameter (D) are nearly the same. A low Reynolds number indicates a small turbulent intensity affecting the breakup of fuel droplets. In addition, bioethanol fuel has a low Weber number $\left(\mathrm{We} = \frac{\rho V^2 D}{\sigma}\right)$ determined by the high surface tension and fuel density, which leads to a slow breakup process. The larger SMD values of bioethanol fuels compared to gasoline fuel can be explained realizing that the calculated breakup lengths of bioethanol fuels are longer than that of gasoline fuel (gasoline: 2.3 ~ 2.5 mm, bioethanol: 5.8 ~ 6.0 mm). In addition, the evaporation of gasoline fuel actively occurs due to its higher vapor pressure compared to bioethanol fuel. On the other hand, the E85 fuel had a similar droplet size as G100. Therefore, bioethanol blended gasoline fuel should

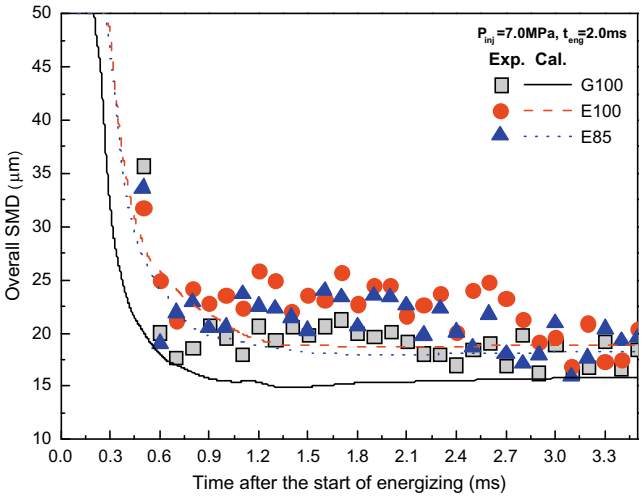

Fig. 9. Comparison of the overall SMD distribution between experimental and calculation results (P_{inj} = 7.0 MPa, P_{amb} = 0.1 MPa, t_{eng} = 2.0 ms).

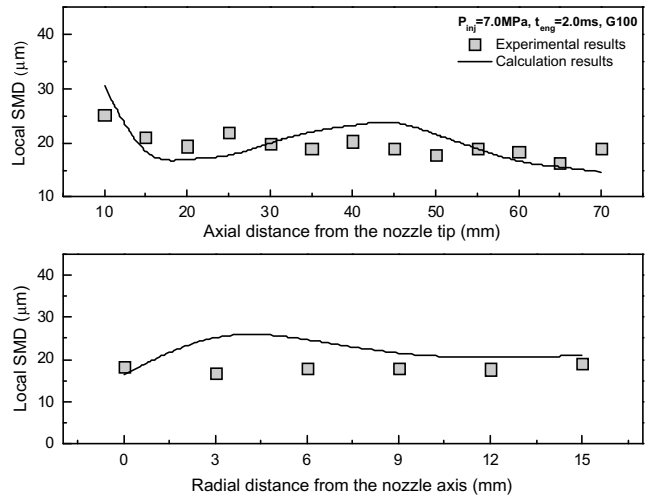

(a) G100

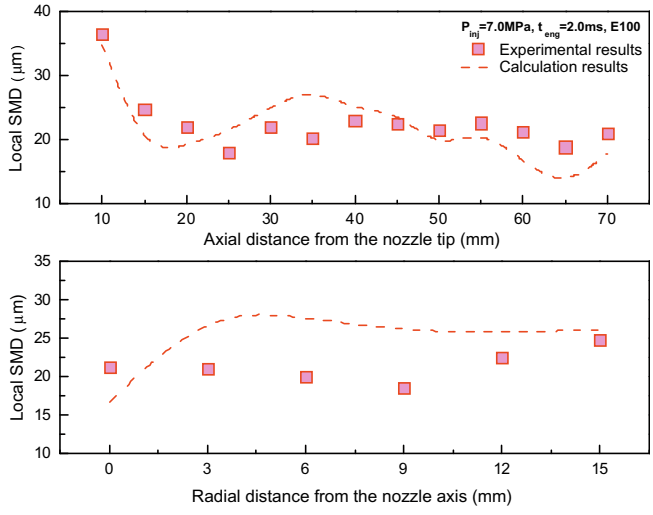

(b) E100

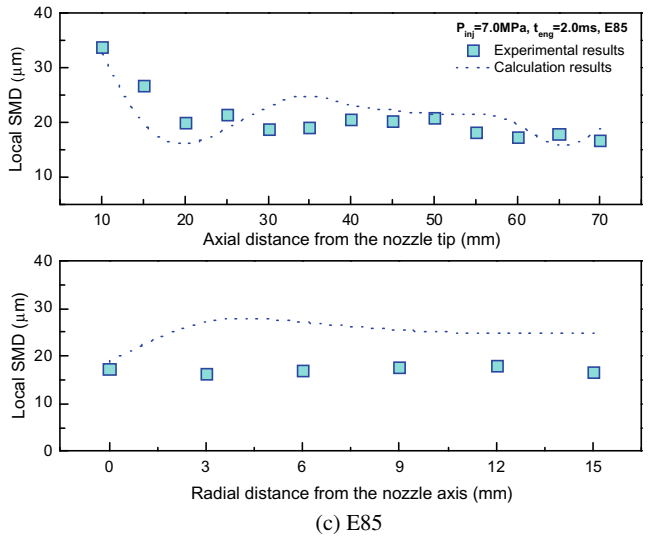

(c) E85

Fig. 10. Comparison of atomization characteristics between experimental and calculation results at the axial and radial direction (P_{inj} = 7.0 MPa, P_{amb} = 0.1 MPa, t_{eng} = 2.0 ms).

be used in a direct injection gasoline engine instead of pure bioethanol fuel. In the local SMD evolution along the radial direction, E100 showed the largest SMD. In addition, the G100 and E85 fuels had almost uniform SMD along the radial distance from the nozzle axis, while the SMD of E100 slightly increased after a radial distance of 9 mm because of collisions and coalescence due to its high kinematic viscosity. The numerical results of the local SMD along the axial distance agree well with the experimental results. However, the predictions in the radial direction were overestimated.

5. Conclusions

In this paper, the spray behavior and atomization performance of gasoline, bioethanol, and bioethanol blended gasoline fuels were investigated in a high pressure swirl injector. In addition, the experimental results were compared with numerical results obtained using the KIVA-3V code.

1. Fuel properties including fuel density, kinematic viscosity, and surface tension of bioethanol blended gasoline fuel increased as the blending ratio of bioethanol fuel, which has high density, kinematic viscosity, and surface tension values, was increased.
2. The upward ring shaped vortex of the three test fuels (G100, E100, and E85) occurred on the surface of the spray 1.1 ∼ 1.2 ms after the start of energizing. In addition, the beginning timings and development processes of the vortices of the test fuels were very similar. The vortex moved the spray droplets to the inside of the hollow cone. This characteristics of the upward ring shaped vortex produced uniform mixture formation and homogeneous distribution of the injected spray.
3. The numerical results well predicted the experimentally observed spray development pattern and shape, the beginning position of the vortex, and spray breakup on the spray surface. In addition, the increase of the injection pressure caused a circular shape of the downstream spray and a uniform mixture between the injected spray droplets and ambient air.
4. The axial spray tip penetrations of the test fuels were similar, while the spray width and spray cone angle of E100 were slightly larger than the other fuels. The increased injection pressure caused an increase of the axial spray tip penetration, also leading to a fast decrease of the spray cone angle after the end of the main spray.
5. The E100 fuel had the largest droplet size among G100, E100, and E85 because E100 has high kinematic viscosity and surface tension values. As confirmed by the size region results of the droplets, E100 had a wider and higher droplet size region than the G100 and E85 fuels.

Acknowledgement

This work was supported by the Second Brain Korea 21 Project in 2008 and a Korea Research Foundation Grant funded by the Korean Government (MOEHRD, KRF-2008-314-D00056).

References

Aleiferis, P.G., Malcolm, J.S., Todd, A.R., Cairns, A., Hoffmann, H., 2008. An optical study of spray development and combustion of ethanol, iso-octane and gasoline blends in a DISI engine. SAE Technical Paper. 2008-01-0073.

Amsden, A.A., 1993. KIVA-3: a KIVA program with block-structured mesh for complex geometries. LA-12503-MS, pp. 33–38.

Chang, W., Kim, Y., Kong, J., 2007. Design and development of a spray-guided gasoline DI engine. SAE Technical Paper. 2007-01-3531.

Dombrowski, N., Johns, W.R., 1963. The aerodynamic instability and disintegration of viscous liquid sheets. Chemical Engineering Science 18, 203–214.

Gao, J., Jiang, D., Huang, Z., 2007. Spray properties of alternative fuels: a comparative analysis of ethanol–gasoline blends and gasoline. Fuel 86, 1645–1650.

Kawahara, N., Tomita, E., Kasahara, D., Nakayama, T., Sumida, M., 2004. Fuel breakup near nozzle exit of high-pressure swirl injector for gasoline direct injection engine. SAE Technical Paper. 2004-01-0542.

Kim, S., Kim, Y., Lee, J., 2008. Analysis of the in-cylinder flow, mixture formation and combustion processes in a spray-guided GDI engine. SAE Technical Paper. 2008-01-0142.

Lee, C.S., Chon, M.S., Park, Y.C., 2001a. Spray structure of high pressure gasoline injector in a gasoline direct injection engine. International Journal of Automotive Technology 2–4, 165–170.

Lee, C.S., Kim, H.J., Park, S.W., 2004. Atomization characteristics and prediction accuracies of hybrid break-up models for a gasoline direct injection spray. Proceedings of IMechE Part D: Journal of Automobile Engineering 218, 1041–1053.

Lee, C.S., Lee, K.H., Chon, M.S., Kim, D.S., 2001b. Spray structure and characteristics of high pressure gasoline injectors for direct injection engine application. Atomization and Sprays 11, 35–48.

Lucchini, T., D'Errico, G., Nordin, N., 2005. CFD modeling of gasoline sprays. SAE Technical Paper. 2005-24-086.

O'Rourke, P.J., Amsden, A.A., 1987. The tab method for numerical calculation of spray droplet break-up. SAE Technical Paper. 872089.

Powell, J.W., Lee, C.F., 2007. An investigation of multiple scattering in a hollow-cone spray. SAE Technical Paper. 2007-01-0648.

Schmidt, D.P., Nouar, I., Senecal, P.K., Rutland, C.J., Martin, J.K., Reitz, R.D., Hoffman, J.A., 1999. Pressure-swirl atomization in the near field. SAE Technical Paper. 1999-01-0496.

Senecal, P.K., Schmidt, D.P., Nouar, I., Rutland, C.J., Reitz, R.D., Corradini, M.L., 1999. Modeling high-speed viscous liquid sheet atomization. International Journal of Multiphase Flow 25, 1073–1097.

Vita, A.D., Allocca, L., 2003. Experimental analysis and CFD simulation of GDI sprays. SAE Technical Paper. 2003-01-0004.

Wang, X., Gao, J., Jiang, D., Huang, Z., Chen, W., 2005. Spray characteristics of high-pressure swirl injector fueled with methanol and ethanol. Energy and Fuels 19, 2394–2401.

Zhao, F., Lai, M.C., Harrington, D.L., 1999. Automotive-spark ignited direct-injection gasoline engines. Progressed in Energy and Combustion Science 25, 427–532.